Draft version July 3, 2023
Typeset using LaTeX **twocolumn** style in AASTeX631

Constraints on the origins of the Galactic neutrino flux

Abhishek Desai,[1] Justin Vandenbroucke,[1] Samalka Anandagoda,[2] Jessie Thwaites,[1] and M.J. Romfoe[1]

[1] *Dept. of Physics and Wisconsin IceCube Particle Astrophysics Center, University of Wisconsin–Madison, Madison, WI 53706, USA*
[2] *Clemson University, Department of Physics & Astronomy, Clemson, SC 29634-0978, USA*

Abstract

Galactic and extragalactic objects in the universe are sources of high-energy neutrinos that can be detected by the IceCube neutrino detector, with the former being easier to resolve due to comparatively smaller distances. Recently, a study done using cascade-like events seen by IceCube reported neutrino emission from the Galactic plane with $>4\sigma$ significance. In this work, we put a limit on the number of Galactic sources required to explain this emission. To achieve this, we make use of a simulation package created to simulate point sources in the Galaxy along with the neutrino and gamma-ray flux emissions originating from them. Along with making use of past IceCube sensitivity curves, we also account for Eddington bias effects due to Poisson fluctuations in the number of detected neutrino events. By making use of a toy-Monte Carlo simulation method, we find that there should be more than 10 sources, each with luminosities 10^{35} erg/s responsible for the Galactic neutrino emission. Our results constrain the number of individual point-like emission regions, which applies both to discrete astrophysical sources and to individual points of diffuse emission.

1. INTRODUCTION

The Milky Way is host to a variety of astrophysical objects, interstellar gas, and radiation fields. By observing the particles created through interactions within and between these phenomena, we can deepen our understanding of the processes involved. While photons from the Milky Way are easily observable -making the Galactic plane the brightest region in the sky- other particles like neutrinos are not so easily observable. Neutrinos can be produced via processes like stellar explosions or supernovae (see e.g. Thompson et al. 2003), the interaction of cosmic rays with matter (Domokos et al. 1993), binary systems with a compact object and a massive star (Levinson & Waxman 2001; Kheirandish 2020) or other sources in our Galaxy. In this work, we study neutrinos in the TeV-PeV regime, which can be produced due to cosmic ray interactions or sources like pulsars and supernova remnants in the Galaxy.

High-energy neutrinos are produced from the decay of charged pions ($\pi^{\pm}$), which are the result of hadronic (pp) or photohadronic ($p\gamma$) interactions. These processes also lead to the production of neutral pions (π^0), which then decay into gamma rays. The gamma-ray emission from the Galactic plane is extremely bright and is studied in the GeV to TeV regime by various observatories like the *Fermi*-LAT (Ackermann et al. 2015; Ackermann et al. 2012), HAWC (Zhou et al. 2018; Albert et al. 2020), HESS (Abdalla et al. 2018), TIBET (Amenomori et al. 2021), LHAASO (Cao et al. 2023), MAGIC (Acciari et al. 2020), VERITAS (Adams et al. 2021) etc. As only hadronic interactions can give rise to both neutrinos and gamma rays, a multi-messenger detection will allow us to investigate the fundamental processes behind these interactions.

The IceCube neutrino observatory is an in-ice cubic kilometer neutrino detector at the South Pole, which detects high-energy neutrinos through their interactions in the ice. Muon neutrino charged-current interactions give rise to muons that are long-lived and travel several kilometers in the ice. On the other hand, short-lived hadronic cascades in the ice can be created through all-flavor neutral current interactions or through electron and tau neutrino charged-current interactions. These interactions in the ice emit Cherenkov radiation that is detected by digital optical modules (DOMs) along strings embedded in the ice. The signals are sent to the IceCube data acquisition system where properties of the event are determined, such as energy, direction, and event morphology: track-like or cascade-like (Abbasi et al. 2009; Aartsen et al. 2017b).

Corresponding author: Abhishek Desai
desai25@wisc.edu

Identification of the production mechanisms and sources of high-energy neutrinos observed by IceCube is one of the prime questions of multi-messenger astrophysics. Recently, Abbasi et al. (2023) (referred to as "DNN cascades" from this point) reported neutrino emission with $> 4\sigma$ significance from the Galactic plane by making use of cascade-like events detected by the IceCube Neutrino Observatory. Detection of this Galactic neutrino signal raises important questions analogous to those posed by the isotropic (extragalactic) neutrino signal. Although there is evidence for two individual extragalactic neutrino sources TXS 0506+056 (Aartsen et al. 2018) and NGC 1068 (Abbasi et al. 2022), they only contribute $\sim$1% (depending on energy) of the total extragalactic signal (Abbasi et al. 2022). Non-detection of a larger number of extragalactic sources constrains the emission to be produced by an abundant population of relatively low-luminosity sources (Abbasi et al. 2022). However, both the number density and luminosity function of the sources as a whole remain unknown, along with the extent to which these quantities evolve with redshift and what the distance scale of typical sources is. For the Galactic neutrino signal, on the other hand, even before determining the nature and origins of the emission, the distance scale and even the approximate large-scale spatial distribution of the emission is well known. This means that the IceCube measurement of the total Galactic neutrino flux is also a measurement of the total Galactic neutrino luminosity. It can also be used to put constraints on the typical luminosity of contributing sources which are directly related not only to the number density of sources but also to the total number of sources in the Galaxy.

Diffuse Galactic neutrino emission is generically expected from cosmic rays interacting with the interstellar medium to produce pions that decay to gamma rays and neutrinos. There are likely also individual astrophysical sources of neutrinos within the Galaxy (Kheirandish 2020). Searches for possible Galactic neutrino emitters using various candidate source lists have been performed, some examples of which include (Aartsen et al. 2017a, multiple Galactic source lists), (Aartsen et al. 2020a, PWN), (Kheirandish & Wood 2020, HAWC Galactic sources), (Abbasi et al. 2022) and (Abbasi et al. 2023, LHASSO sources). No significant emission has been found, and all these studies placed upper limits on the neutrino flux from Galactic sources. However, the total Galactic flux reported in Abbasi et al. (2023) is several times higher than predicted by models of diffuse emission, indicating that discrete sources may provide an important component of the flux. For particular Galactic source lists tested in Abbasi et al. (2023), the source lists cannot be distinguished from one another, nor from the diffuse scenario, because the IceCube cascade sample has relatively large ($\sim$7°) angular resolution and the large-scale spatial distribution of the emission is very similar in the various scenarios. Because of the spatial similarity, constraints on the luminosity and number of Galactic sources can be constructed robustly, with a weak dependence on the exact spatial distribution. In this work, we present a simulation package to estimate the neutrino (and gamma-ray) contribution from individual Galactic sources and use it to draw conclusions from the results presented by Abbasi et al. (2023).

This work is divided as follows. Sec. 2 describes a simple limit on the number of sources contributing to the neutrino signal without the use of any simulation. Sec. 3 explains the simulation package and how it works. In Sec. 4, we discuss how the package can be used to simulate gamma-ray source populations, comparing them to detected sources. In Sec. 5, we use the simulation to determine a lower limit on the number of sources or emission sites for Galactic neutrinos. This is done by estimating the number of Galactic sources or neutrino emission points that can be detected by IceCube, the conclusions for which are explained in Sec 6.

2. NEUTRINOS FROM THE GALACTIC CENTER

We start with a simple assumption that all neutrino sources responsible for the DNN cascades detection are collected at the center of the Galaxy and are point sources. The KRA_γ^{50} (Gaggero et al. 2015) best-fit flux reported by DNN cascades can then be approximated as the total neutrino flux from the Galactic center. The best-fit flux for the KRA_γ^{50} template at 100 TeV is given by $\sim 1.5\times10^{-15}\,\mathrm{TeV}^{-1}\mathrm{cm}^{-2}\mathrm{s}^{-1}$ (Fig. 5 of Abbasi et al. 2023). Next, we use the sensitivity and 4σ discovery potential curves for the DNN cascade sample and sensitivity and 5σ discovery potential curves for the 10-year point source tracks sample (Aartsen et al. 2020b, referred to as "PS tracks" from this point). While sensitivity gives the 90% CL (confidence level) upper limit when the Test Statistic (TS) equals 0, the $4(5)\sigma$ discovery potential shows the flux required to detect the source at $4(5)\sigma$. Assuming all the neutrino sources at the Galactic center are responsible for the total measured $\sim 1.5\times10^{-15}\,\mathrm{TeV}^{-1}\mathrm{cm}^{-2}\mathrm{s}^{-1}$ flux and have a value equal to these sensitivity and discovery potential curves, the number of sources contributing to the signal are shown in Table. 1. Note that we use "flux" in this work to denote the differential neutrino number flux at 100 TeV in units of $\mathrm{TeV}^{-1}\mathrm{cm}^{-2}\mathrm{s}^{-1}$ unless specified otherwise.

Table 1. Number of sources (N_{src}) making up the measured best-fit total Galactic neutrino flux assuming all sources are point sources located at the center of the Galaxy (at ∼-28° declination) and have flux values given by the sensitivity and discovery potential (DP) curves from the DNN cascades (DNN) and PS tracks (PST) work. The flux spectrum (dN/dE) proportional to E^{-2} and E^{-3} is tested for both cases. As no Galactic neutrino sources have been detected, these can be viewed as lower limits on the number of such sources.

Sample Tested	$E^{-2.0}$ Flux at ∼-28°	N_{src} ($E^{-2.0}$)	$E^{-3.0}$ Flux at ∼-28°	N_{src} ($E^{-3.0}$)
DNN sensitivity	1.05×10^{-16}	14	6.19×10^{-17}	24
DNN 4σ DP	3.26×10^{-16}	5	1.97×10^{-16}	8
PST sensitivity	2.25×10^{-16}	7	3.29×10^{-15}	0
PST 5σ DP	7.97×10^{-16}	2	1.37×10^{-14}	0

We can already see from this simple test that because of the improved sensitivity of the DNN cascades sample in the Southern hemisphere, it has a better chance of detecting neutrinos from the Galactic center. However, because the localization is better for track events (less than 1° for ∼100 TeV events; see Abbasi et al. 2021a) compared to cascade events (∼ 7° at 100 TeV, see Abbasi et al. 2023), it would be difficult to resolve the sources, even if they are detected. In other words, source confusion would be a serious challenge if the sources are tightly clustered at the Galactic center. On the other hand, if they are sufficiently clustered, then they could be detected as an aggregate excess (perhaps spatially extended) above the surrounding diffuse emission.

A more robust way to perform this test is to simulate sources in our Galaxy and use the DNN cascades and PS tracks results to see if any of the samples have a chance of detecting them. We perform this study by using the simulation code described below.

3. *SNUGGY*

The simulation package created to simulate point-like Galactic sources is named "*Simulation of the Neutrino and Gamma-ray Galactic Yield*" (*SNuGGY*) and is made available on Desai et al. (2023). This package is analogous to an existing simulation tool called FIRESONG (Tung et al. 2021), which simulates extra-galactic gamma-ray and neutrino sources. The main functioning of the code can be divided into two parts, explained in the subsections below.

3.1. *Simulating Source Positions*

The core logic to simulate the Galactic source population is to use the two-dimensional probability distribution function (PDF) of the number density of Galactic sources in Galactocentric coordinates. This can either be a simple two-dimensional exponential PDF (identified as "exponential" below) or a modified two-dimensional exponential PDF mimicking a more realistic distribution (identified as "modified_exponential" below). If the location of the source with respect to the center of the Galaxy is given by R and the vertical height above the Galactic plane is given by z, the two number densities mentioned above are given by the following equations:

- For the exponential setup, the 2D PDF is given by

$$\rho(R, z) = \rho_0 \, e^{-\frac{R}{R_0}} \, e^{-\frac{|z|}{z_0}} \tag{1}$$

  where ρ_0 is the normalization parameter, R_0 and z_0 are the scale length and scale height, respectively. For the example here, we use the same parameters as the ones used by Winter et al. (2016) for the millisecond pulsar distribution and are given by $R_0 = 3$ kpc and $z_0 = 0.6$ kpc. Note that while determining the R and z PDFs, the Jacobian is included.

- For the modified_exponential setup, the 2D PDF is given by

$$\rho(R, z) = \rho_0 \left(\frac{R}{R_\odot}\right)^{\alpha} exp\left(-\beta \frac{R - R_0}{R_\odot}\right) exp\left(-\frac{|z|}{h}\right) \tag{2}$$

  where, α, β, h are again parameters for the distribution. This equation is taken from Ahlers et al. (2016) where the α, β, and h parameters for the pulsar distribution (2, 3.53, 0.181) shown by Lorimer et al. (2006) and supernova remnant distribution (1.93, 5.06, 0.181) by Case & Bhattacharya (1998) are used as reference. Fig. 3.1 shows the 2D histogram using the parameters for the pulsar distribution case. Note that the vertical distance (r) peaks at a value away from the center of the Galaxy as expected from the Jacobian factor and agrees with pulsar distribution studies like Yusifov & Kucuk (2004).

These PDFs are converted to inverse cumulative distribution functions, which are then used to sample a given number of sources (the PDF sampling method used is similar to Tung et al. 2021). For now, only the two above-mentioned setups exist in the framework, with the possibility of adding more in the future if required.

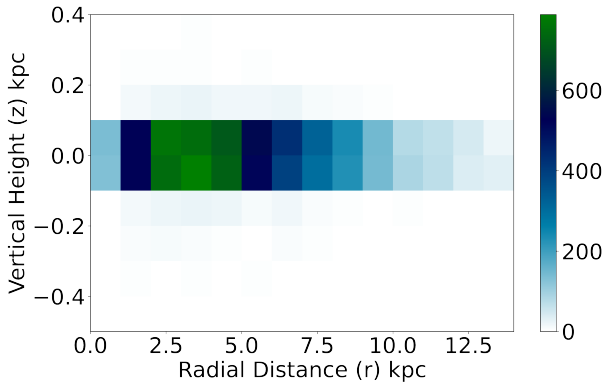

Figure 1. 2D Histogram showing the simulated vertical height (z) and distance (R) with respect to the center of the Galaxy for a set of 10^4 sources. Note that this is the result of one simulation while making use of the modified exponential distribution function described in Sec 3.1, along with the pulsar distribution parameters.

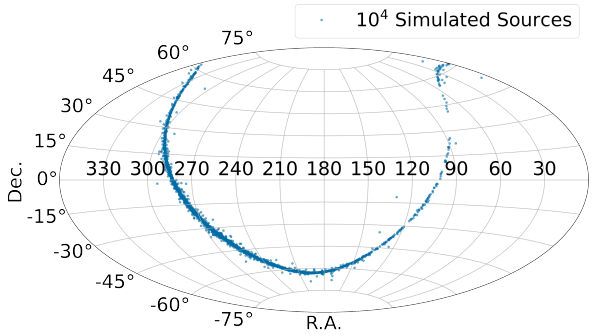

Figure 2. Simulated source positions in equatorial coordinates. Note that this is the result of one simulation of the modified exponential distribution function described in Sec 3.1.

Both existing frameworks simulate a disk Galaxy with the Galactic bulge and thickness depending on the specified input parameters. Fig 2 shows the simulated sources for the above-mentioned simulation in the International Celestial Reference System (ICRS) coordinates.

3.2. *Deriving Flux Estimates*

Next, we simulate the observed neutrino flux for every source. This is done by assigning the integrated neutrino luminosity (over 10 TeV-10 PeV, and in units of erg/s) of the source and using the distance and spectrum to derive the flux, assuming a simple power-law spectral model. Note that we use the word "luminosity" from this point to denote integrated luminosity over 10 TeV-10 PeV unless specified otherwise. To get the luminosity, either a standard candle (SC) approach is used where all sources have equal luminosity, or a log-normal (LN) distribution is used and described below:

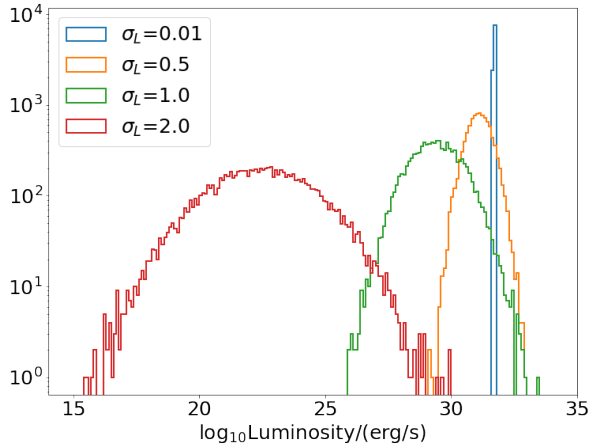

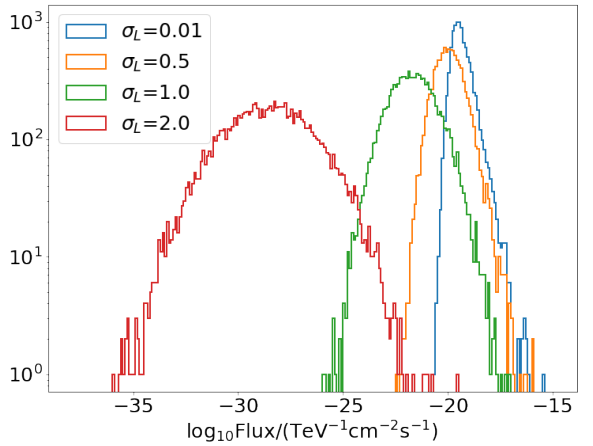

Figure 3. Top: Luminosity distribution for sources simulated using the Log Normal Luminosity method. The mean luminosity in this example is calculated by making use of Eq. 4 where the total flux is fixed to 2.18×10^{-15} TeV^{-1}. For a low value σ_L=0.01, the distribution behaves like a standard candle where all source luminosities are close to the mean. Bottom: Corresponding flux distribution for the simulated sources using luminosities shown in the top plot. The flux values are energy differential at 100 TeV and are simulated based on the luminosity distributions shown in top panel, an index of 2.0, a energy range of 0.1-100 TeV, and source positions shown in Fig. 2.

- Standard Candle Luminosity: For a set of N simulated sources, we assign the simulated distance,

d_i, for each source, i. Let the total Galactic flux be given by $\phi_{Galactic}$ and L_{SC} be the standard candle luminosity per source. Assuming that the luminosity of each source is the same and sources are centered on the Galactic center ($\sim$ 8 kpc; Leung et al. 2022), the standard candle luminosity is given by

$$L_{SC} = \frac{\phi_{Galactic}}{\frac{N}{4\pi(8kpc)^2}} \quad (3)$$

This method ensures that the standard candle luminosity is selected such that the sum of fluxes per source, derived using L_{SC} and d_i, is close to the total Galactic flux $\phi_{Galactic}$. To derive the differential flux from the integrated luminosity, a power law spectrum with an index γ is used over an energy range given by E_{min} and E_{max}, where all these parameters are used as inputs to the simulation. This method includes cosmic variance, which varies the total Galactic flux for each simulation while keeping the luminosity per source fixed and is called the "StandardCandle" approach in the simulation code.

- Forced Standard Candle Luminosity: We also give a special case of simulating standard candle sources using the "Forced_standardCandle" mode in the code. For this forced case, the sum of simulated fluxes is exactly equal to the Galactic diffuse flux $\phi_{Galactic}$. L_{SC}, in this case, is simulated by:

$$L_{SC} = \frac{\phi_{Galactic}}{\sum_{i=1}^{N} \frac{1}{4\pi d_i^2}} \quad (4)$$

Note that this method is similar to the previous approach, but the actual simulated distance per source is used in the calculation instead of a fixed value of 8 kpc. Due to this difference, the previous method will cause the total simulated flux to be close to but not equal to the input $\phi_{Galactic}$.

- Log Normal Luminosity: This method is the most realistic setup to simulate luminosities. It uses a probability density function (PDF) similar to the one described by Dinsmore & Slatyer (2022). Using an input value of the mean luminosity L_0 in erg/s, the PDF can be given by

$$P_{LN}(L) = \frac{log_{10}e}{\sigma_L L\sqrt{2\pi}} exp\left(\frac{-(log_{10}L - log_{10}L_0)^2}{2\sigma_L^2}\right) \quad (5)$$

where the σ_L parameter controls the width of the distribution. Giving a very low σ_L value will result in a simulated distribution where all the luminosities equal the mean luminosity, i.e. a standard candle approach (see Fig 3. In the event that a mean luminosity value is not specified as an input, the code uses the forced standard candle approach (equation. 4) to first find the mean luminosity.

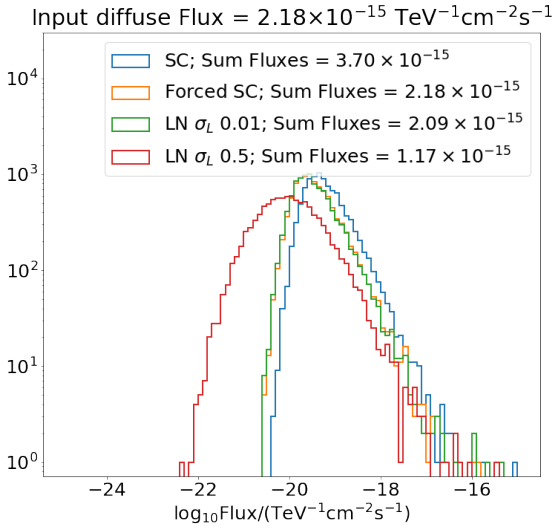

Figure 4. Flux distribution for 10^4 sources simulated using different estimation techniques. The total sum of the simulated fluxes is also shown in the legend to compare to the input given for the total Galactic flux measurement of 2.18×10^{15}(Abbasi et al. 2023).

A comparison of the flux estimated using all three methods for one simulation of 10^4 sources is shown in Fig. 4. The total Galactic flux derived is also shown in the legend and matches exactly for the forced standard candle case. Note that for log-normal cases, the mean luminosity (L_0) is set to "None" so that the code uses an approach similar to eq. 4 to estimate L_0. A low value of σ_L like 0.01 (as shown in the figure) will thus simulate a source population mimicking a "standard candle" approach. For the log-normal with higher σ_L, a more realistic scenario of the sum of fluxes not equaling the diffuse flux is seen.

These flux estimation methods can be used for simulating both neutrino and gamma-ray fluxes for sources. While features in the *SNuGGY* code have been added to simulate gamma-ray fluxes from neutrino fluxes (and vice versa) using $pp/p\gamma$ interactions (Kelner et al. 2006; Halzen 2022), neutrino and gamma-ray fluxes can also be simulated separately. This avoids relying on a model-dependent scenario where all neutrinos and gamma-rays

are related by $pp/p\gamma$ interactions. In this work we simulate the gamma-ray and neutrino fluxes individually.

4. GALACTIC GAMMA-RAY SOURCES

The *SNuGGY* package can be used to simulate gamma-ray fluxes using the methods shown in Sec. 3.2. To test the validity of the code setup, we make use of the "Log Normal Distribution" method and compare it with existing gamma-ray observations of pulsar and pulsar-associated sources. While the source position distributions we use for the simulation follow a pattern similar to PWN (Pulsar Wind Nebula) sources, we are actually just simulating point sources using *SNuGGY*. This would mean we can compare observations of other pulsar source classes like millisecond pulsars (MSPs) provided that the source positions and luminosities are accounted for in the simulations.

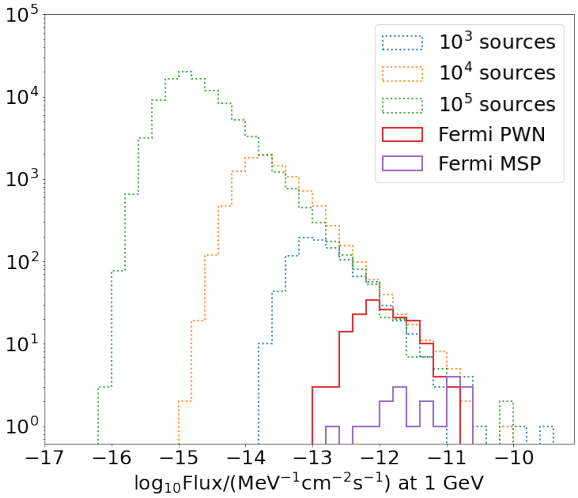

Figure 5. Point sources simulated using the *Fermi*-LAT Galactic diffuse flux measurement at 1 GeV in units of MeV^{-1}cm^{-2}s^{-1} (only for this comparison) along with a σ_L of 0.01 are shown using the dotted lines. The sum of all simulated fluxes equals 10^{-9}MeV^{-1}cm^{-2}s^{-1}. Flux estimates from the *Fermi*-LAT 4FGL-dr3 catalog for PWN and MSP sources are also shown using solid lines.

We first simulate sources with the condition that the total simulated flux equals the total Galactic diffuse gamma-ray flux without specifying the mean luminosity. The total Galactic diffuse gamma-ray flux is estimated at 1 GeV using the model taken from Ackermann et al. (2015) and given by 10^{-9} MeV^{-1}cm^{-2}s^{-1}. Using a σ_L value of 0.01, we simulate a standard candle distribution of different numbers of sources (points of gamma-ray emission). The flux distribution of these simulations is then compared to the observations reported in the *Fermi*-LAT 4FGL-dr3 catalog (Abdollahi et al. 2022) for PWN and MSP sources. The observed sources fall on the bight end of the simulated source distribution (see Fig. 5), highlighting the potential of using the *SNuGGY* framework for similar source population studies. Note that, for this sample case, we do not simulate a specific source class of pulsars but just a distribution of gamma-ray points in the Milky Way.

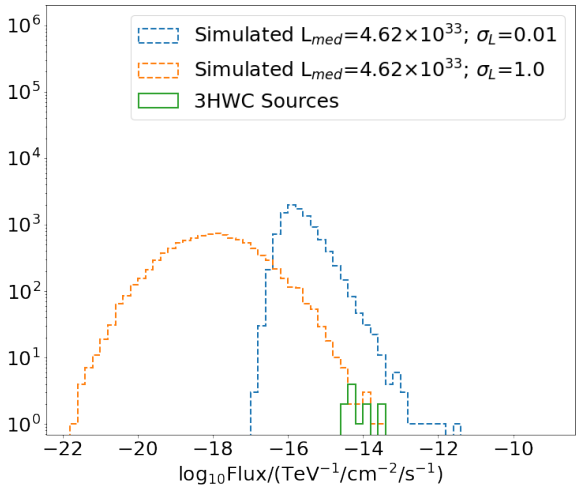

Figure 6. Sources simulated using the observations reported in the 3HWC catalog are shown for σ_L of 0.01 and 1.0. The derived differential flux simulations, at an energy of 7 TeV, are shown by dashed lines, while the 11 3HWC source observations (with TeV halo candidate pulsars within 1°) are shown as solid lines. The integrated luminosity over 0.1-100 TeV derived using the 3HWC observations is used as an input in this case, so the total flux estimate is not fixed. Note that, as the integrated luminosities derived from the 3HWC catalog are spread out, a higher value of σ_L is preferred where the actual observations move towards the brighter end of the simulated histogram.

We also use higher energy (∼7 TeV) observations of 11 sources seen by the HAWC telescope and reported in the 3HWC catalog (Albert et al. 2020). As the HAWC catalog reports observations for HAWC sources with corresponding TeV halo candidate pulsars within 1° of the observations, we make use of the reported estimated luminosity values. For this case, we use the mean luminosity of ∼4.6×10^{33} erg/s (integrated over the energy range of 0.1 to 100 TeV) derived from the 3HWC catalog by making use of the reported flux measurements and distances given in Tables 2 and 4 of Albert et al. (2020). The simulated 10^4 source flux distributions for

a σ_L value of 0.01 and 1.0 are shown in Fig. 6), as compared to the reported HAWC observations at 7 TeV. The estimated luminosity for the 3HWC sources varies from $\sim 1\times10^{31}$ to $\sim 1\times10^{35}$ erg/s while the mean luminosity is $\sim 4.6\times10^{33}$ erg/s. This would mean that the luminosities follow a distribution similar to a log normal distribution with a high σ_L value. Using this in the simulation brings the simulation closer to the real scenario where the 3HWC sources should lie on the bright end of the histogram (see Fig. 6).

5. GALACTIC NEUTRINO SOURCES ANALYSIS

We use the *SNuGGY* framework to simulate these Galactic neutrino sources of varying number densities and luminosities to better understand results like Abbasi et al. (2023) which search for Galactic neutrinos. All reported luminosities for the neutrino studies are integrated luminosities over 10 TeV-10 PeV, while the fluxes (simulated and taken from Abbasi et al. 2023) are differential measurements at 100 TeV. We test two cases for the source position: All simulated sources at the center and simulated sources following a PWN distribution simulated using α, β, and h equals 2, 3.53, 0.181 (Lorimer et al. 2006). Note that the spatial distribution of other Galactic neutrino source classes is similar to the PWN distribution allowing us to make conclusions about Galactic neutrino source classes as a whole using this study. We derive the neutrino fluxes for these sources based on the *SNuGGY* framework. Once the sources are simulated with a corresponding neutrino flux, they are compared to the sensitivity and discovery potential curves from the IceCube samples (DNN cascades and PS tracks) to check whether the simulated flux is above the threshold for a source to be detected by IceCube. A source is considered to be detected if the simulated flux value is higher than the sensitivity or discovery potential value. This is shown as an example in Fig. 7, where one simulation of 10^4 neutrino sources and their fluxes is computed and shown as the blue data points and compared to the IceCube sensitivity curves. If the simulated flux is above the sensitivity curve, it shows that the neutrino sample is sensitive to neutrinos coming from that simulated source and will result in detection with a TS greater than the median TS. However, a comparison with the 4σ (5σ) discovery potential curves (instead of sensitivity) will allow us to find simulated sources that can be detected with a significance that is higher than 4σ (5σ).

5.1. *Eddington Bias*

We also account for Eddington bias while estimating the number of detected sources by accounting for Poisson fluctuations in the number of neutrinos per source.

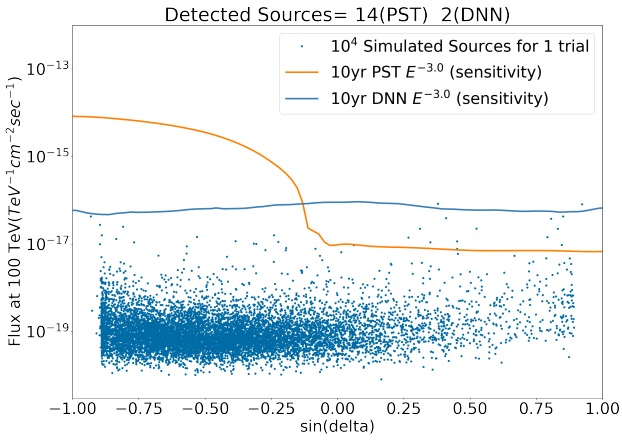

Figure 7. Comparison of simulated sources with the 90% CL sensitivity curves from the IceCube PS tracks and DNN cascade data samples. Blue points show 10^4 simulated sources with fluxes derived using a log-normal luminosity distribution with σ_L=0.01 (distribution mimics a standard candle approximation). If a simulated source flux is above the sensitivity curve, the source is counted as detected.

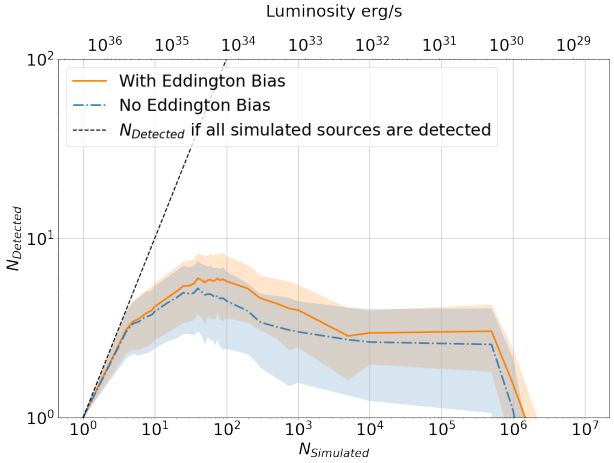

Figure 8. Change in the number of detected sources after inclusion of Eddington bias is shown here. Note that the number of detected sources increases in the low-luminosity and high source-number regime because of fluctuations in the number of detected events due to Eddington bias.

As described by Strotjohann et al. (2019), Eddington bias is the bias seen when upward Poisson fluctuations in the number of neutrinos detected from a source cause an overestimation of the source flux. This bias can be particularly large when there are many dim sources. We add Poisson fluctuations to the number of neutrino events expected per simulated source to account for this. Using the effective area curves reported by Abbasi et al.

(2021a) (IC86v2; for PS tracks) and by Abbasi et al. (2023) (Figure 2 of paper; for DNN cascades), we estimate the number of expected neutrino events, over a period of 10 years, depending on the simulated source flux. Note that for this calculation, we make the approximation that the effective area curves of the DNN cascade sample do not change with declination. While the number of events would change as the declination changes, especially at higher energies, the change is not significant in our analysis and would only modify the uncertainty in the cases of a large number of simulated sources due to more sources being simulated across the Galactic plane and not just close to the center.

The number of expected neutrino events also changes as a function of energy because of the power law index of the neutrino spectrum and the dependence of effective area on neutrino energy. So the total neutrino event counts, integrated over energy, are used, which is then Poisson fluctuated to account for Eddington bias effects. The fluctuated events are compared with a threshold number of events required for detection, which is derived using the sensitivity or discovery potential flux. The number of detected sources for this setup varies as compared to a simple no-bias setup, as shown in Fig. 8. More sources for the low-luminosity scenario are detected after the addition of Eddington bias, bringing the simulation closer to the real-world scenario.

5.2. *Toy-MC setup*

Using this procedure to simulate sources and compare them to IceCube sensitivities, we simulate multiple source populations with varying numbers of simulated sources. As the input total diffuse flux is kept constant for these cases, the few source sample is made up of highly luminous sources, while the larger source samples are made up of lower luminosity sources. We also report the mean luminosity as a function of the number of simulated sources which can be used to put limits on the source population. Using the above method to simulate the sources and after accounting for Eddington bias (see Sec. 5.1), the number of sources detected is calculated for each case. This is repeated multiple times (at least 1000) to give a mean number of detected sources along with a 1σ uncertainty. For the cases being tested, we use the sensitivity curves from both the PS tracks samples and the 5σ (4σ) discovery potential curves from the PS tracks (DNN) samples. We test the scenarios with the neutrino flux (dN/dE) proportional to a power law, with spectral indices of 2.0 and 3.0.

5.3. *Case 1: All sources are at the Galactic center*

As a test, we simulated sources at the Galactic center and used them to see how the IceCube sensitivity curves compare with them. To achieve this, the simple exponential approach described in Eq. 1 is used with R_0 value equal to 0. We then simulate the per-source fluxes by making use of the "Log Normal Luminosity" with a σ_L=0.01 using the method described in Sec. 3.2. The mean luminosity, in this case, is not specified, allowing the code to estimate it using the method described by equation. 4. Note that this ensures that the mean luminosity changes depending on the number of sources simulated, allowing us to test populations with a few high-luminosity sources vs. a large number of low-luminosity sources). The flux distribution is computed once the mean luminosity is estimated based on the value of a given σ_L. The results of this test are shown in Fig. 9. Note that the results seen for this simulation case come close to the ones shown in Table. 1. This confirms the validity of the simulation method used here.

5.4. *Case 2: Sources simulated in a more realistic scenario*

For this case, a more realistic distribution (the "modified exponential", described in Sec. 3.1) is used to simulate neutrino source locations The fixed parameters, α=1.93, β=5.06, and h=0.181 are used as reported by Ahlers et al. (2016) for the Lorimer et al. (2006) pulsar wind nebula (PWN) distribution. We also test the parameters for the Case & Bhattacharya (1998) supernova remnant distribution (α=2, β=3.53 and h=0.181 kpc), but the final results are very similar to the pulsar distribution case, so we only report the PWN distribution here.

The flux estimation follows a procedure similar to Sec. 5.3, but with a σ_L value equal to 0.01 (standard candle distribution) and σ_L=0.5 (test case to include broader luminosity functions). See Fig. 3 to see how the simulated luminosities and fluxes change with a change in σ_L. The results for this case in terms of the number of sources detected by IceCube are shown in Figs. 10 and 11. Note that the number of sources detected heavily depends on the shape of the sensitivity/discovery potential curve used for comparison. For less than 10 sources, almost all of the sources are detected using the DNN cascades event sample.

5.5. *Angular Resolution (source confusion)*

Note that the simulations described above do not account for the angular resolution of the event samples and only check to see if a point source is bright enough to be significant in the IceCube event sample used. This would mean that source confusion effects are not included, and sources that are significant in both the tracks and cascade sample will be noted as "detected" regardless of separation from one another. While the DNN

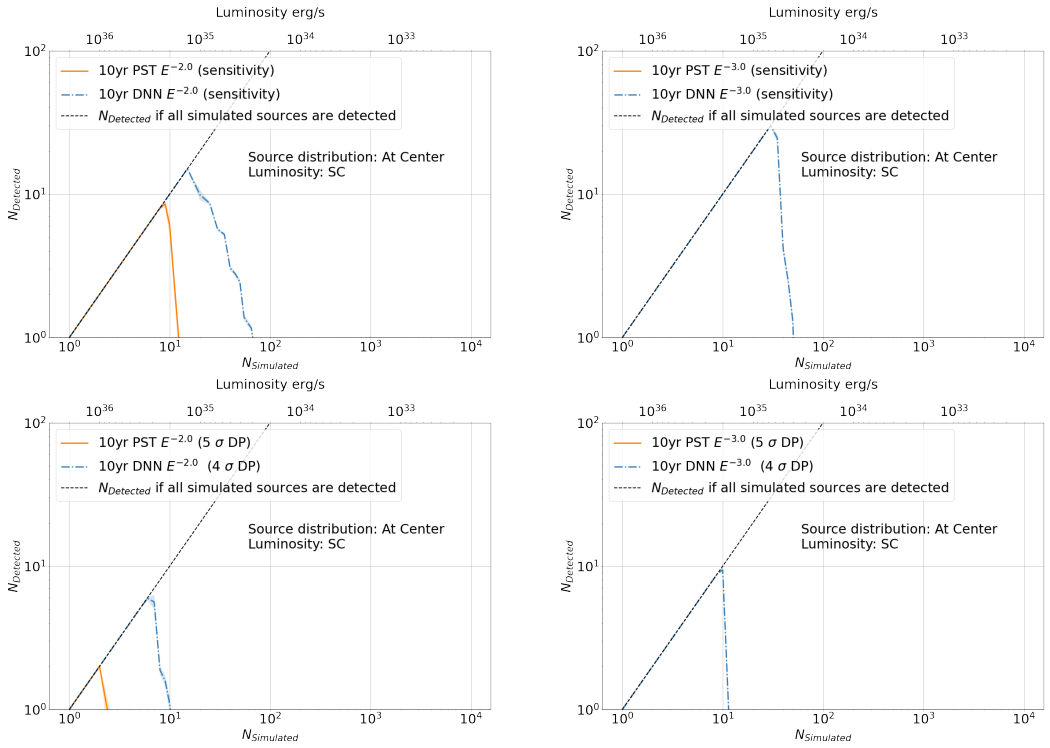

Figure 9. Special case for sources simulated at the Galactic center: The number of detected neutrino sources at the Galactic center for different sensitivity and discovery potential curves while using a σ_L=0.01 TeV^{-1}cm^{-2}s^{-1}. The top row makes use of sensitivity curves, while the bottom row makes use of discovery potential curves. On the left is index=2.0, and right is index= 3.0. The shaded regions show the $\pm 1\sigma$ uncertainty.

cascades sample has better sensitivity in the Southern hemisphere as compared to PS tracks, the angular resolution is poor as compared to the tracks sample (see Abbasi et al. 2023, for more details). Another IceCube dataset is currently under development with ∼10 years of starting tracks events as reported by Silva & Mancina (2020); Abbasi et al. (2021b). As can be seen from Abbasi et al. (2021b), the shape of the sensitivity curve of this enhanced starting tracks event sample (ESTES) is similar to the cascades sample but with a different scaling. In other words, the sample is equally sensitive in the Northern and Southern hemispheres. This would imply that the shape of the number of detected ($N_{Detected}$) curves for DNN cascades shown in Figs. 9- 11 as blue dashed lines will be similar for ESTES but scaled according to the sensitivity of the ESTES sample.

To test the dependence of our results on angular resolution, we simulate a set of N number of sources similar to Sec 5.4 and find the minimum angular separation between the simulated sources. This is done ∼100 times to get the mean minimum separation between sources and associated standard deviation. We compare this to the reported angular uncertainty estimates at 100 TeV for: DNN cascades (given by $\sim 7^\circ$ for all events; see Abbasi et al. 2023), PS tracks (given by $\sim 0.3^\circ$; see Abbasi et al. 2021a) and ESTES (assumed to be 1.0°). This is used to find the number of sources the IceCube event samples will be able to resolve based on the mean simulated minimum separation angle curve. We find that DNN cascades will be able to resolve $N \sim 5$ sources using the all events sample, PS tracks will be able to resolve $N \sim 26$ sources, while ESTES will be able to resolve $N \sim 13$ sources.

6. GALACTIC NEUTRINO SOURCES DISCUSSION

Using the results shown in Sec. 5.3 - 5.5, we can come to the following conclusions in relation to the Galactic neutrino contributions:

- **Galactic Center Sources**: The DNN cascades sample has a better chance of detecting bright neutrino sources at the Galactic center as compared to PS tracks (see Fig. 9). However, in the case of detection, it will be difficult to resolve many sources detected by the cascade sample. The results derived using this test match the ones shown in Table 1 while the simulation rules out the possibility of a small number of very bright sources making up the signal. Additionally, in case of no detection using the DNN cascades, this scenario can be ruled out. Additionally, this result is solidified

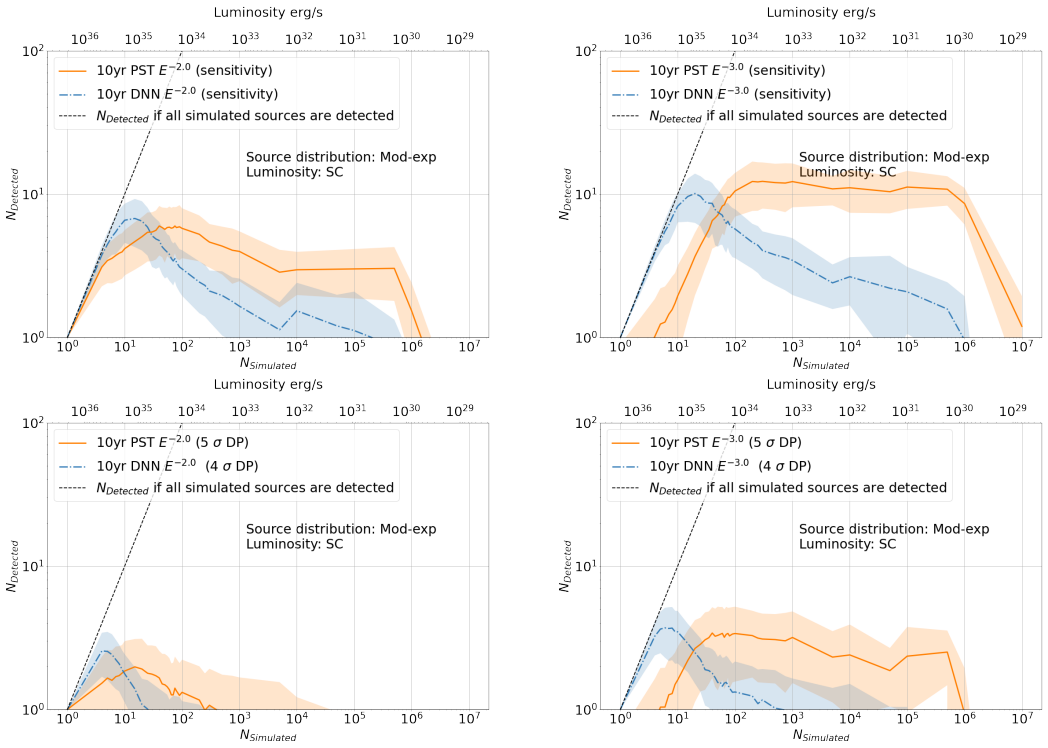

Figure 10. Case for sources simulated with a realistic geometric distribution (Modified exponential distribution dubbed as "Mod-exp" here) and a standard candle approach for fluxes: Number of detected neutrino sources for different sensitivity and discovery potential curves while using a σ_L=0.01 and total diffuse flux equals 2.18×10^{-15} TeV^{-1}cm^{-2}s^{-1}. The 2.18×10^{-15} is obtained using the best-fit neutrino flux derived for the DNN cascade sample using the π^0 template (Abbasi et al. 2023) The top row makes use of sensitivity curves, while the bottom row makes use of discovery potential curves. On the left is index=2.0 and right is index= 3.0. The shaded regions show the 1σ uncertainty.

when effects due to angular resolution (Fig. 12) are included.

- **Number of neutrinos per source:** The angular separation test shown in Sec. 5.5 assumes that sources are resolvable if separated by the median angular resolution of the event sample. Depending on the event selection and source spectrum, detecting a source in a decade or more of integration (and therefore background) requires $O(10)$ neutrino events from the source, which means that the localization of individual detected sources is actually better than the single-event angular resolution and this requirement is conservative. This means that the DNN cascades analysis, for example, would be able to individually resolve more than five detected point sources if they were from a population following a typical Galactic spatial distribution.

- **Lower limit on the number of Galactic neutrino sources**: The discovery potential comparisons show that if the Milky Way were to have just a few neutrino sources of comparable luminosity producing the total measured flux, the DNN cascades analysis would have detected them. As shown in Table. 2, for particular parameter choices, this lower limit on the number of sources is even stronger. The limit is weaker only for a spectral index of 2.0 and log-normal luminosity case. This is expected for populations with large luminosity variance. As the total number of Galactic sources increases, the mean luminosity decreases, and fewer sources would be detected with the DNN cascades event sample. This holds true even after including fluctuations due to Eddington bias, which increases the number of detected sources in the regime of many low-luminosity sources. To put a conservative limit on the number of detected sources using the DNN cascades sample, we use the SC scenario with a modified exponential distribution (Column 2 in Table 2). For an index of 2.0, the value equals 26 sources. Using the lower limit of $N_{Detected}$ instead of the mean to find the point when $N_{Detected} = 1$ changes this value to $\sim$ 10 (see Fig. 10: Bottom Left panel). Using these results from our simulation study and the

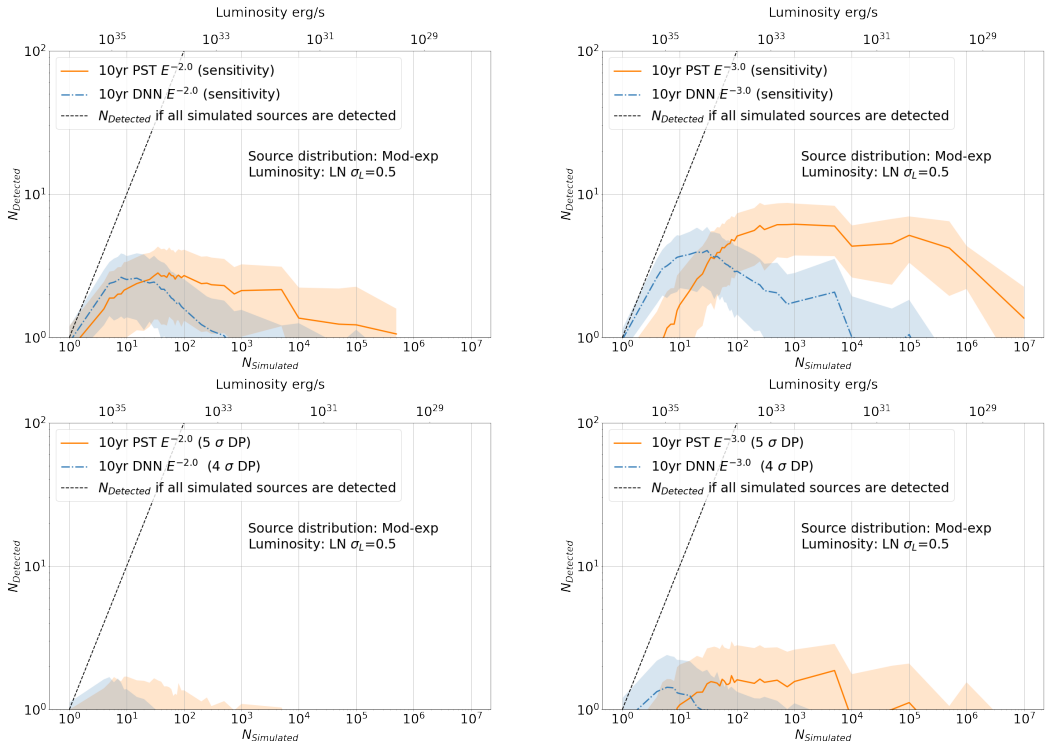

Figure 11. Case for sources simulated with a realistic geometric distribution (Modified exponential distribution dubbed as "Mod-exp" here) and a log-normal approach for fluxes: Number of detected neutrino sources for different sensitivity and discovery potential curves using σ_L=0.5 and total flux equals 2.18×10^{-15}. The top row makes use of sensitivity curves, while the bottom row makes use of discovery potential curves. On the left is index=2.0 and right is index= 3.0. The shaded regions show the 1σ uncertainty.

Table 2. Lower limit on the approximate number of sources detected by the DNN cascades sample based on the simulations are shown here (mean value of $N_{Detected}$ in Figs 9-11 marked by blue dashed line). The upper limit on the mean luminosities is also given. This is found by noting the maximum number of simulated sources (dashed line showing the mean value in Figs 9-11 for the DP case) required to detect at least 1 source.

Quantity	SC ($\sigma_L = 0.01$)	LN ($\sigma_L = 0.5$)	Sources at center
$N_{src}(\gamma = 2.0)$	26	0	10
$L_{mean}(\gamma = 2.0)$	$3.9{\times}10^{34}$	-	$1.9{\times}10^{35}$
$N_{src}(\gamma = 3.0)$	672	29	12
$L_{mean}(\gamma = 3.0)$	$1.2{\times}10^{33}$	$1.1{\times}10^{34}$	$1.6{\times}10^{35}$

fact the Abbasi et al. (2023) was not able to detect any sources, we can conclude that there are $\gtrsim$ 10 sources making up the diffuse signal with a mean luminosity of 10^{35} erg/s of the sample.

7. CONCLUSION

This work describes the *SNuGGY* simulation code, which can be used to simulate Galactic point sources along with their neutrino and gamma-ray fluxes. The diversity of the analyses that can be performed using the code is shown, along with a focus on using the simulation to draw robust conclusions from the recent IceCube Abbasi et al. (2023) detection of the Galactic neutrino flux. Using a Monte-Carlo simulation performed for Galactic neutrino sources, we determine lower limits on the number of Galactic sources contributing to the observed flux. As the distribution of different Galactic source classes follows a similar pattern, simulations presented here can be applied to different Galactic source classes and even be used as points of neutrino emission in the Galaxy due to cosmic rays interacting with matter. Non-detection of any individual Galactic neutrino source to date (Aartsen et al. 2020a; Abbasi et al. 2022; Kheirandish & Wood 2020; Abbasi et al. 2023; Abbasi et al. 2023), combined with the total flux normalization measured by IceCube, enables us to determine that there must be more than ∼10 individual sources (or points of diffuse emission), each with luminosity 10^{35} erg/s, producing the signal.

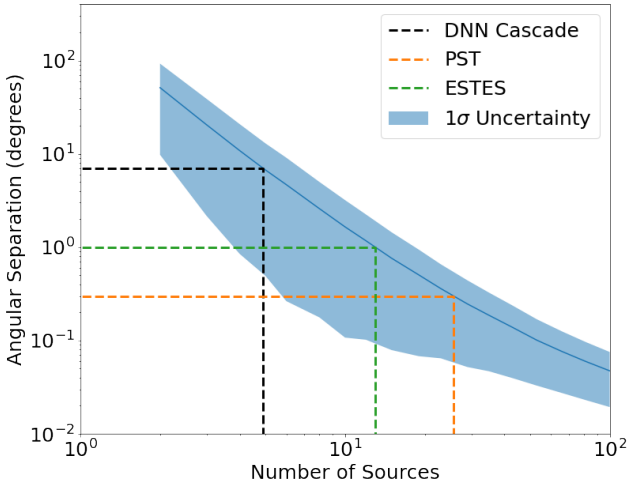

Figure 12. Comparison of the minimum separation angle of different number of simulated sources with the angular resolution of IceCube event samples at 100 TeV. The shaded region shows the 1σ uncertainty, and the dashed and dotted lines show the minimum number of sources the IceCube event samples will be able to resolve.

8. ACKNOWLEDGEMENTS

The authors would like to thank the members of the IceCube Collaboration for their valuable suggestions. The authors would also like to thank Markus Ahlers for helpful discussions relating to the spatial distribution of the Galactic sources, Alex Pizzuto for helping with the initial development of the *SNuGGY* code, and Aswathi Balagopal and Sam Hori for discussions related to the result. A. Desai is supported by a John Bahcall Fellowship at the Wisconsin IceCube Particle Astrophysics Center (WIPAC) at the University of Wisconsin-Madison. J. Vandenbroucke is supported by a Vilas Associate award at the University of Wisconsin-Madison.

REFERENCES

Aartsen, M. G., et al. 2017a, Astrophys. J., 849, 67
—. 2017b, JINST, 12, P03012
—. 2018, Science, 361, eaat1378
—. 2020a, Astrophys. J., 898, 117
—. 2020b, PhRvL, 124, 051103
Abbasi, R., et al. 2009, Nucl. Instrum. Meth. A, 601, 294
—. 2021a, arXiv:2101.09836
—. 2021b, PoS, ICRC2021, 1130
—. 2022, arXiv:2210.04930
Abbasi, R., et al. 2022, Science, 378, 538
Abbasi, R., et al. 2022, Astrophys. J. Lett., 930, L24
Abbasi, R., et al. 2023, Science, 380, 1338
Abbasi, R., et al. 2023, Astrophys. J. Lett., 945, L8
Abdalla, H., et al. 2018, Astron. Astrophys., 612, A1
Abdollahi, S., et al. 2022, Astrophys. J. Supp., 260, 53
Acciari, V. A., et al. 2020, Astron. Astrophys., 642, A190
Ackermann, M., et al. 2012, ApJ, 750, 3
Ackermann, M., et al. 2015, Astrophys. J., 799, 86
Adams, C. B., et al. 2021, Astrophys. J., 913, 115
Ahlers, M., et al. 2016, Phys. Rev. D, 93, 013009
Albert, A., et al. 2020, Astrophys. J., 905, 76
Amenomori, M., et al. 2021, Phys. Rev. Lett., 126, 141101
Cao, Z., et al. 2023, arXiv:2305.05372
Case, G. L., & Bhattacharya, D. 1998, Astrophys. J., 504, 761
Desai, A., Vandenbroucke, J., & Anandagoda, S. 2023, doi:10.5281/zenodo.8092198; https://github.com/abhishekdesai90/SNuGGY/tree/v0.0.0
Dinsmore, J. T., & Slatyer, T. R. 2022, JCAP, 06, 025
Domokos, G., Elliott, B., & Kovesi-Domokos, S. 1993, Journal of Physics G: Nuclear and Particle Physics, 19, 899
Gaggero, D., et al. 2015, Astrophys. J. Lett., 815, L25
Halzen, F. 2022, Int. J. Mod. Phys. D, 31, 2230003
Kelner, S. R., Aharonian, F. A., & Bugayov, V. V. 2006, Phys. Rev. D, 74, 034018, [Erratum: Phys.Rev.D 79, 039901 (2009)]
Kheirandish, A. 2020, Astrophys. Space Sci., 365, 108
Kheirandish, A., & Wood, J. 2020, PoS, ICRC2019, 932
Leung, H. W., et al. 2022, Monthly Notices of the Royal Astronomical Society, 519, 948
Levinson, A., & Waxman, E. 2001, Phys. Rev. Lett., 87, 171101
Lorimer, D. R., et al. 2006, Mon. Not. Roy. Astron. Soc., 372, 777
Silva, M., & Mancina, S. 2020, PoS, ICRC2019, 1010

Strotjohann, N. L., Kowalski, M., & Franckowiak, A. 2019, Astron. Astrophys., 622, L9

Thompson, T. A., Burrows, A., & Pinto, P. A. 2003, Astrophys. J., 592, 434

Tung, C. F., et al. 2021, J. Open Source Softw., 6, 3194

Winter, M., et al. 2016, Astrophys. J. Lett., 832, L6

Yusifov, I., & Kucuk, I. 2004, Astron. Astrophys., 422, 545

Zhou, H., Rho, C. D., & Vianello, G. 2018, PoS, ICRC2017, 689